Article

Large-Scale Ligand Perturbations of the Protein Conformational Landscape Reveal State-Specific Interaction Hotspots

Timothy R. Stachowski and Marcus Fischer*

Read Online

ACCESS | 📊 Metrics & More | 📖 Article Recommendations | 🔲 Supporting Information

ABSTRACT: Protein flexibility is important for ligand binding but often ignored in drug design. Considering proteins as ensembles rather than static snapshots creates opportunities to target dynamic proteins that lack FDA-approved drugs, such as the human chaperone, heat shock protein 90 (Hsp90). Hsp90α accommodates ligands with a dynamic lid domain, yet no comprehensive analysis relating lid conformations to ligand properties is available. To date, ~300 ligand-bound Hsp90α crystal structures are deposited in the Protein Data Bank, which enables us to consider ligand binding as a perturbation of the protein conformational landscape. By estimating binding site volumes, we classified structures into distinct major and minor lid conformations. Supported by retrospective docking, each conformation creates unique hotspots that bind chemically distinguishable ligands. Clustering revealed insightful exceptions and the impact of crystal packing. Overall, Hsp90α's plasticity provides a cautionary tale of overinterpreting individual crystal structures and motivates an ensemble-based view of drug design.
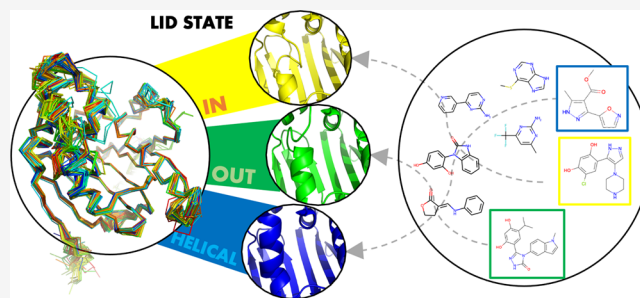
◼ INTRODUCTION

Baffled by the complexity of targeting dynamic proteins, ligand discoverers often treat protein structures as static objects.[1,2] This common practice conveniently reduces the complexity of targeting a multitude of dynamic states,[3] but it ignores key aspects of ligand binding.[4−6] Proteins accommodate ligands in various ways, two of which have been popularized.[7] First, the "conformational selection" paradigm suggests that ligands can bind and stabilize pre-existing conformations that proteins adopt[8] even in the apo state.[2,9,10] Second, the "induced fit" paradigm suggests that the protein optimizes complementarity through additional adjustments,[11] either locally or allosterically.[12,13] Describing the dynamics of ligand binding by using these contrasting concepts remains controversial because, in practice, they are often inseparable.[14,15] Again, these concepts represent an attempt to break down the complexity of molecular recognition into approaches we can leverage for ligand discovery.

A more recent, comprehensive approach is to conceptualize protein dynamics[16] as a conformational energy landscape.[17,18] The energy-landscape concept captures both discrete states and energy barriers to traverse them.[19] From a methods standpoint, the energy landscape is typically explored using complementary approaches, such as molecular dynamics simulations,[20] crystallography,[21] single-molecule Förster resonance energy transfer,[22] hydrogen−deuterium exchange mass spectrometry,[23] nuclear magnetic resonance,[24] solution X-ray scattering,[25] and more recently, cryo-electron microscopy[26] and X-ray free electron laser experiments.[27] Together, these

methods cover functional protein motions on a breadth of timescales.[17] In lieu of explicit dynamic data, an exploration of protein conformational ensembles can be achieved by systematically perturbing the energy landscape via changes in temperature,[28,29] pH,[30,31] humidity,[32,33] electric field pulses,[34] or pressure.[35]

Here, we consider ligands as a perturbation of the protein conformational landscape.[36] Ligand binding reshapes the protein conformational ensemble by destabilizing certain states while stabilizing others.[5,37] This often includes local changes in sidechain rotamers or collective motions like loop repositioning.[38] Typical structure-based ligand-discovery campaigns produce individual structural snapshots upon developing new compounds. Over time, these efforts culminate into large datasets of ligand-perturbed structures that illuminate the protein conformational landscape. One particularly rich structural dataset is that of human heat shock protein 90 alpha (Hsp90α), a dynamic molecular chaperone that facilitates cell homeostasis by assisting protein folding.[39,40] Because of its role in facilitating the overexpression of growth and signaling proteins that are associated with all 10 hallmarks
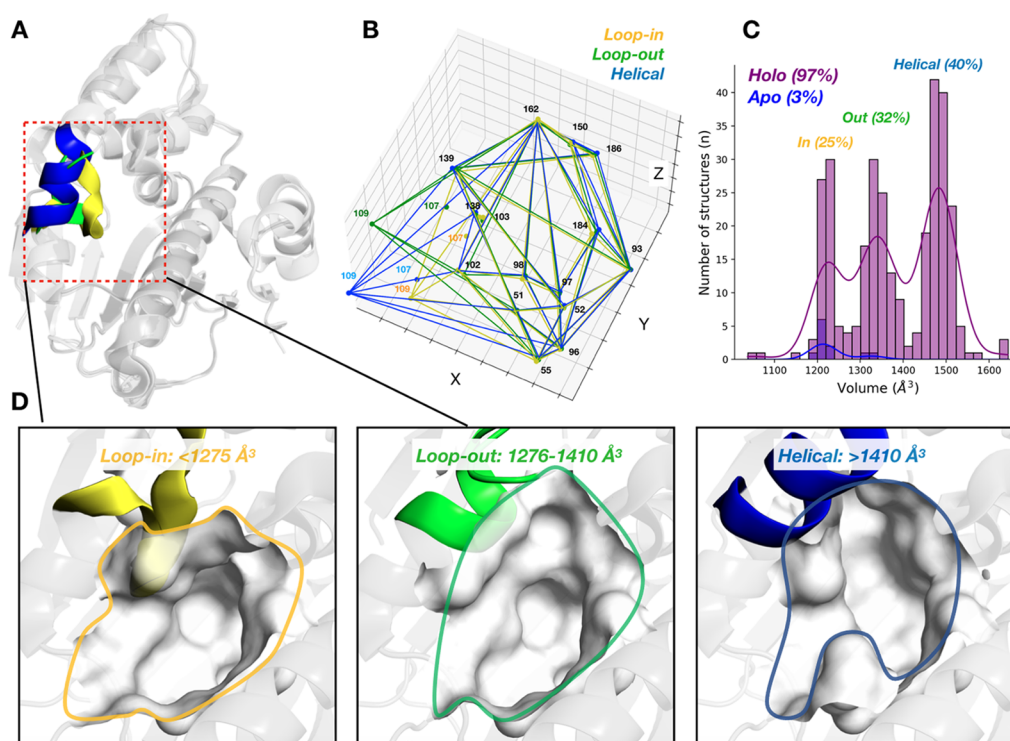
Figure 1. Distinct lid conformations accommodate ligand binding to Hsp90α-NTD. (A) Overview of the Hsp90α-NTD structure. (B) Convex hull (envelope) of the Hsp90α-NTD binding site between the three major states of lid conformations. (C) Distribution of binding-site volumes shows that structures fall into three major groups: loop-in (yellow), loop-out (green), and helical (blue). Ligand binding expands the binding site compared to that in apo structures that populate only the two small-volume groups, loop-in (82%) or loop-out (18%). (D) Ribbon diagrams of representative structures from the three lid conformations (loop-in: 5M4E, loop-out: 3OW6, and helical: 5J27). Inset labels show the volume cutoffs used to determine classifications. See SI, Figure S6 for minor states.

of cancers,[41] inhibiting Hsp90α is a promising strategy to prevent tumor progression.[42] Since rearrangements in the N-terminal domain (NTD) following ATP hydrolysis trigger the conformational cascade that drive client folding and maturation,[43] the ATP-binding site is primarily targeted for inhibition. The site adjacent flexible lid segment, composed of two helices interrupted by a loop,[44] enables chemically diverse ligands to bind.[45] Early evidence of lid flexibility comes from apo structures that showed the lid in "open" and "closed" states between crystal forms.[46] The substrates ATP and ADP both bind the open state.[44,47] The open state is also seen in structures with ansamycin-based ligands like geldanamycin[46] and 17-DMAG.[48] A third conformation in which the lid forms a continuous helix and exposes a hydrophobic pocket has been observed in inhibitor-bound human Hsp90α structures.[49] Like in Hsp90α, this conformation also occurs in human Hsp90β[49] but not in Trap1 and Grp94 isoforms, where it is believed to be less energetically favorable.[50] While some ligands bind independently of the lid conformation,[51] these examples highlight the close connection between ligand binding and flexibility, which varies across Hsp90 isoforms despite high sequence similarity.

The conformation of the lid determines the accessibility of ligands to different regions of the binding pocket.[52] Over the past 25 years, medicinal chemistry has tried to exploit this and produced 300 structures of Hsp90α-NTD bound to drug candidates or fragments in the Protein Data Bank (PDB).[53] Despite this rich structural dataset, comparative studies tend to consider too few conformational states or ligands[54−58] and may miss the bigger picture. No Hsp90α inhibitor has received

FDA approval thus far. One reason might be that relying on individual models to detect contrasting features between isoforms insufficiently captures aspects that are important for developing isoform-specific inhibitors.[52] One limitation to leveraging large structural information is that a comprehensive framework to describe disparate structural data is missing. While a "catch-all" approach is not trivial and general tools to interrogate such data are lacking,[59] recent explorations of the kinase[60] and Ras[61] conformational landscapes demonstrate the value of a large-scale approach.

To more comprehensively characterize Hsp90's targetable conformational landscape, we sought to connect distinct Hsp90α-NTD lid conformations to discernible ligand chemical properties. To enable this, we unified 300 diverse structural datasets by calculating their binding-site volumes. We found that the Hsp90α lid conformations fall into three clearly distinguishable main states: "loop-in", "loop-out", and "helical." In addition, we observed three minor states that are rarely populated by ligands but are distinct from the major states. Each of these conformations creates distinct ligand-binding hotspots that are currently unappreciated when simplifying the system. The crystallographic data are reinforced by retrospective docking that shows that ligands binding each conformation have distinguishable chemical properties and provides additional insights into ligand recognition and discovery. Hierarchical clustering identifies interesting cases, where related ligands stabilize different loop conformations with different poses. Our analysis of crystallographic space groups suggests a connection between crystal-packing preferences and loop conformations that misdirects interpre-
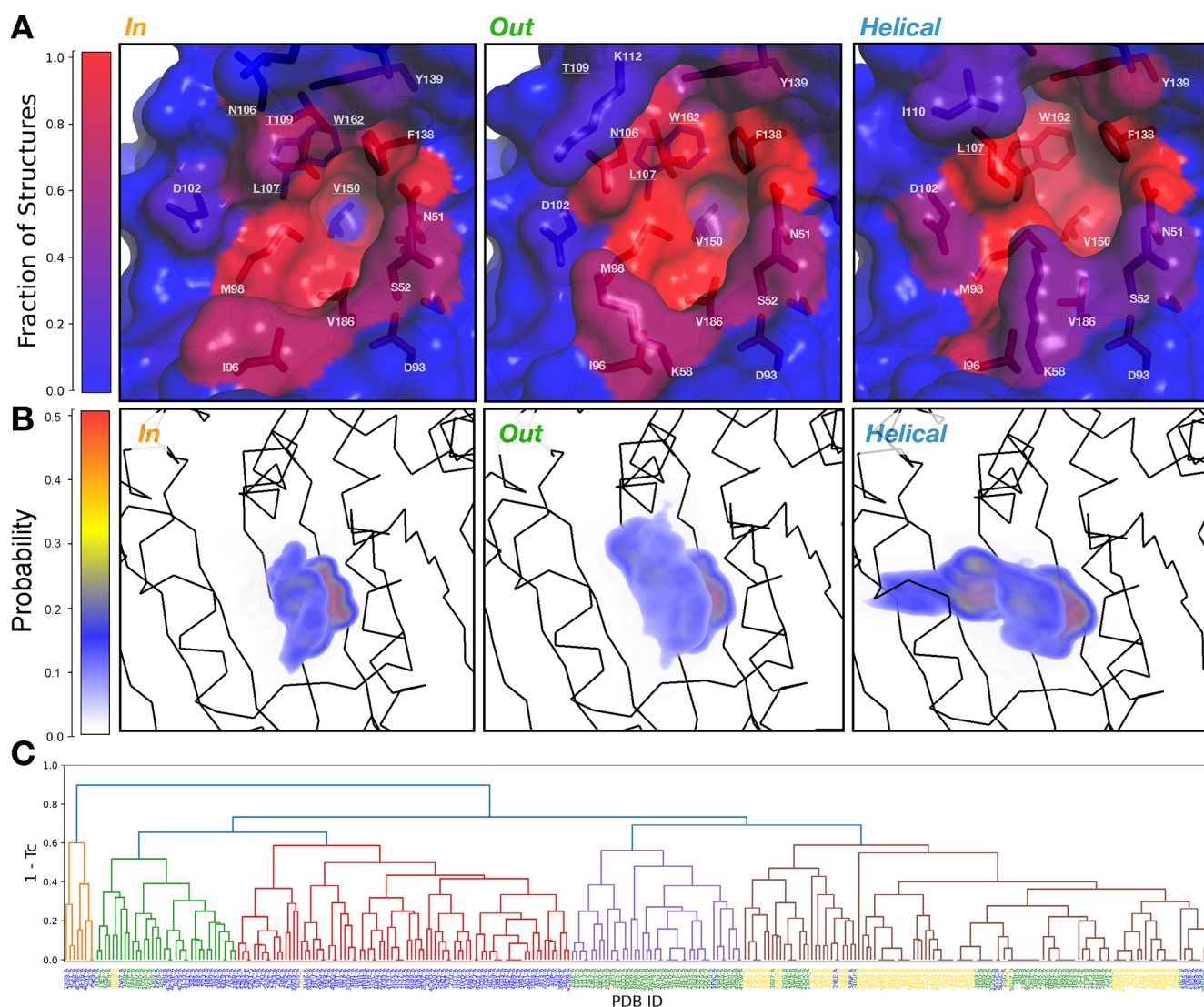
Figure 2. Distinct lid conformations create unique ligand-binding hotspots. (A) Mapping the fraction of structures with residues ≤5.0 Å of a ligand bound to each conformation onto representative PDB structures (loop-in: 5M4E, loop-out: 3OW6, helical: 5J27) shows that T109 is adjacent to fewer ligands in the helical conformation and W162 and V150 are more exposed in the helical conformation. (B) Probability distribution of ligand atoms bound to the three conformations (left: loop-in, center: loop-out, and right: helical). (C) Hierarchical clustering of structures based on Tc similarities of ligand-adjacent residues (protein−ligand fingerprints) shown in (A). Structure IDs are colored by loop conformation (yellow: loop-in, green: loop-out, and blue: helical).

tations of protein−ligand interactions. This work provides a methodological framework for moving from a static to an ensemble understanding of how ligand binding perturbs the conformational landscape of dynamic proteins when many individual structures are available but the relationship is hiding in plain sight.

■ RESULTS

Hsp90α Ligands Bind Three Major and Three Minor Distinct Lid Conformations. Ligand-bound Hsp90α-NTD structures often display varying lid conformations. Three conformations have been observed anecdotally but are not often considered together in comparative studies (Figure 1A). To determine whether this three-state model captures all Hsp90α-NTD structures, we analyzed the binding site of 321 Hsp90α-NTD crystal structures deposited in the PDB. We first confirmed that the quality of the dataset is high for the majority of modeled ligands and lid residues, where map

coefficients are available: 98% of ligands and 94% of lid residues have a real space correlation coefficient (RSCC) of ≥0.8 (SI, Figure S1). All but 11 structures were ligand-bound; common crystallization additives were excluded so that only ligands of biological interest were considered for analysis. We characterized binding-site conformations by estimating the volume of a convex hull (or envelope) around alpha carbon (Cα) atoms that formed the border of the binding site (Figure 1B). In two dimensions, the process is analogous to the shortest perimeter created by releasing a rubber band around a set of points on a plane. The approach is fast and reference-free, and other implementations have been successful for characterizing ligand-binding sites.[62] The volume estimation revealed three discrete populations of lid conformations: loop-in (25%), loop-out (32%), and helical (40%) (Figure 1C,D and SI, Figure S2). Notably, apo structures populated only the two small-volume groups loop-in (82%) and loop-out (18%), indicating that ligand binding typically expands the binding
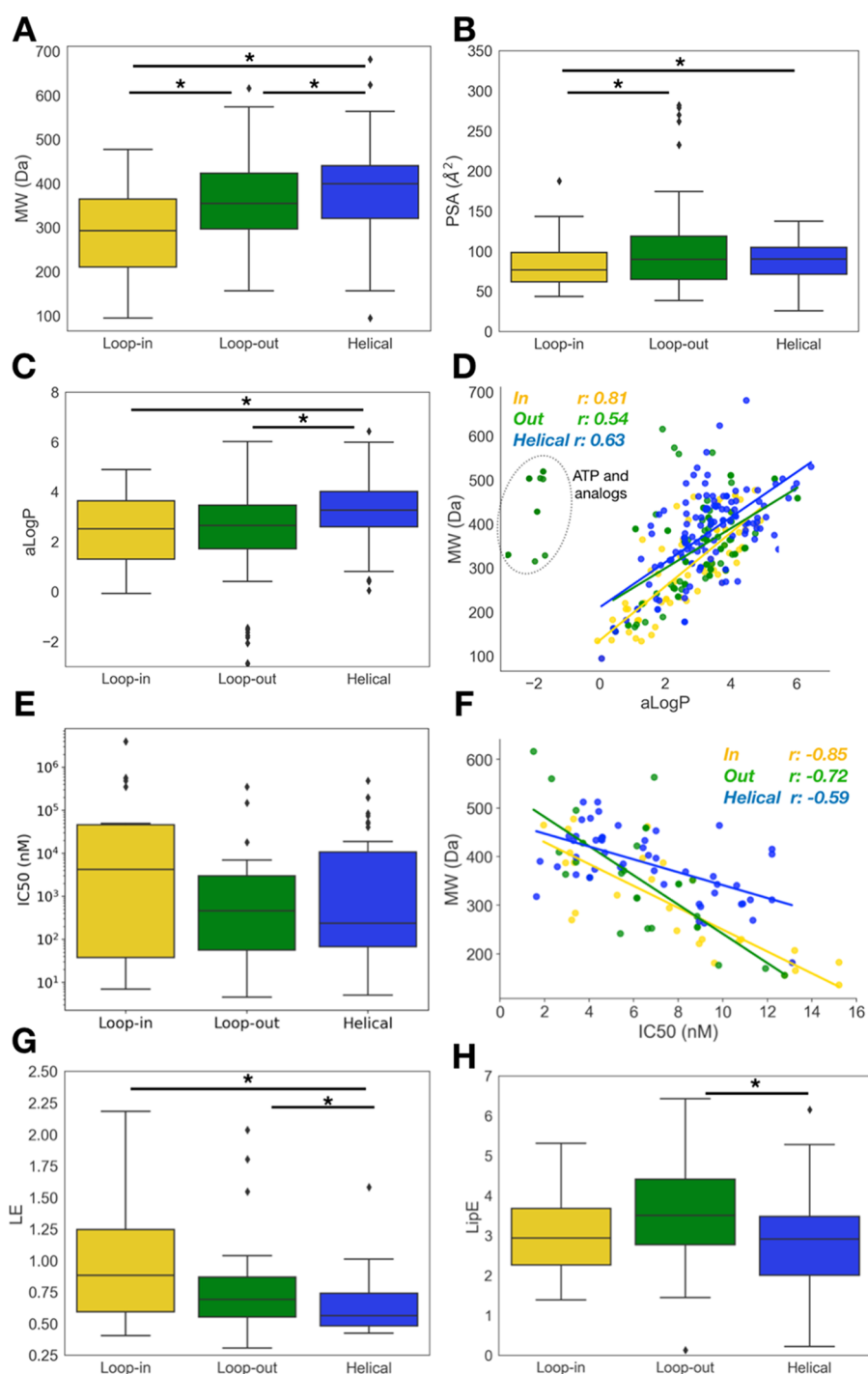
Figure 3. Ligands bound to each conformation exhibit distinct chemical properties. (A) Molecular weight (MW), (B) topological surface area (PSA), and (C) aLogP comparisons between ligands bound to each lid conformation (yellow: loop-in, green: loop-out, and blue: helical). (D) Relation between MW and aLogP among ligands. Data were fitted to a linear regression (excluding ATP and analogues in the dotted oval), where r is the Pearson correlation coefficient. (E) IC_{50} values for 115 ligands available in the PDB. (F) Relations between MW and the log of affinity. (G) Ligand efficiency (LE) and (H) lipophilic efficiency (LipE) of ligands bound to each conformation. LE was caclulated according to LE = | 1.4(− $logIC_{50}$)/N|, where N is the number of non-hydrogen atoms. LipE was calculated according to LipE = pIC_{50} − aLogP where p is the negative log. Asterisks (*) indicate statistically significant comparisons, where *$p < 0.05$ (Mann−Whitney).

site. This expansion drives lid residues Leu107 and Thr109 away from the binding site and creates the helical group (Figure 1D). Although this approach showed that lid conformations can be simplified into three distinct groups, conformational heterogeneity remained within each group. This heterogeneity was most apparent in the loop-out

conformation, both in the structural alignment of all structures within each state (SI, Figure 2B) and when calculating the mean deviation (MDev),[63] a measure of atomic positional fluctuation (SI, Figures S3,S4). Regions showing lid variability agreed across states but varied in intensity. Notably, the binding lid segment (residues 107−115) was more variable in
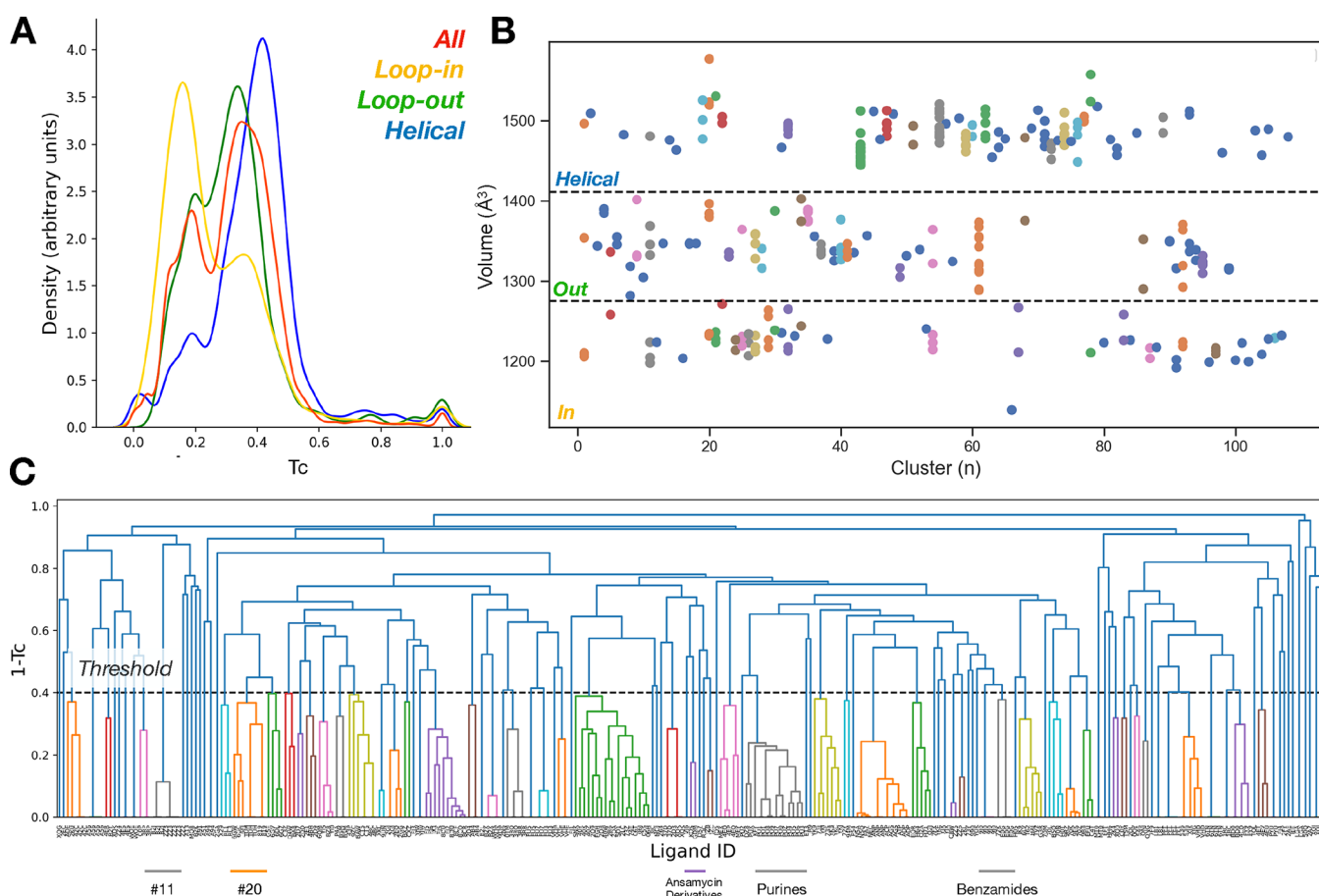
Figure 4. Related ligands often stabilize similar loop conformations. (A) Pairwise Tanimoto coefficients (Tc) consider all ligands (red) or ligands in each lid conformation separately (yellow: loop-in, green: loop-out, and blue: helical). Ligand families were determined by hierarchical clustering with a Tc threshold value of 0.6. (B) Relations between clusters and ligand-binding pocket volumes shows that similar ligands generally bind the same lid conformation, with some notable exceptions highlighted in Figure 5. (C) Clustering dendrogram that produced clusters in (B) showing Tc values where ligand families diverge; several notable classes of inhibitors are highlighted.

the helical than in the loop-in conformation, and the proximal loop (residues 123−127) was more variable in the loop-in conformation (SI, Figure S4). Aside from the overall increased variability of the lid in the loop-out conformation, several loops far from the ligand-binding site were also more variable (SI, Figure S3) and might reflect allosteric effects.[64]

Besides the three major conformations, we identified three distinct minor states that were each present in <1% of the 321 structures. First, we identified populations with volumes of <1100 or >1600 Å³, which are outside the ranges of the major states. We excluded the small-volume binding-site cluster due to apparent modeling errors (SI, Figure S5); however, the large-volume cluster revealed two distinct helical states in which critical residues like Leu107 were oriented differently. One state was populated by three structures and the other was populated by only one structure, 5J86 (SI, Figure S6). Second, despite falling into the volume distribution for the helical state, one additional minor state with three structures was clearly separable from the rest of the volume-clustered structures (SI, Figure S6). Together, these results showed that our categorization of the Hsp90α-NTD binding site can distinguish lid conformations, which are best described as three major and three minor states. Subsequent analyses focused on major states with sufficient structures to extract large-scale trends rather than presenting anecdotal examples. Nonetheless,

our retrospective docking showed that rare states serve as interesting computational starting points for drug discovery.

Distinct Lid Conformations Create Unique Ligand-Binding Hotspots. The position of the lid controls the accessibility of ligands to certain regions of the binding site.[58] To extract general, state-specific binding hotspots, we probed whether the three major lid conformations form distinct binding-site surfaces. To find such hotspots, we calculated how often residues occurred within 5 Å of ligands bound to each lid conformation (Figure 2). This revealed that the involvement of several residues changed as ligands bound to distinct lid conformations. Notably, loop-in and loop-out conformations, which are typically treated as a single conformation, did not share the same binding-site surface. Specifically, lid residue Asn106 was adjacent to 82% of ligands in the loop-out conformation but only to 6% of ligands in the loop-in state. In contrast, Thr109 was adjacent to 68% of ligands in the loop-in state but only near 4% in the loop-out state (SI, Figure S7). Folding Thr109, Ile110, and Ala111 into the helical state created a new cleft that exposed Trp162 almost exclusively (87%) to helical binders (Figure 1D and SI, Figure S7). Lid repositioning in the helical conformation also created a flat surface on the binding-site floor that made Val150 more accessible (90%) than in the loop-in (23%) or loop-out (51%) conformations. Alternatively, we visualized the probability distribution of atoms in ligands for each state to show that each
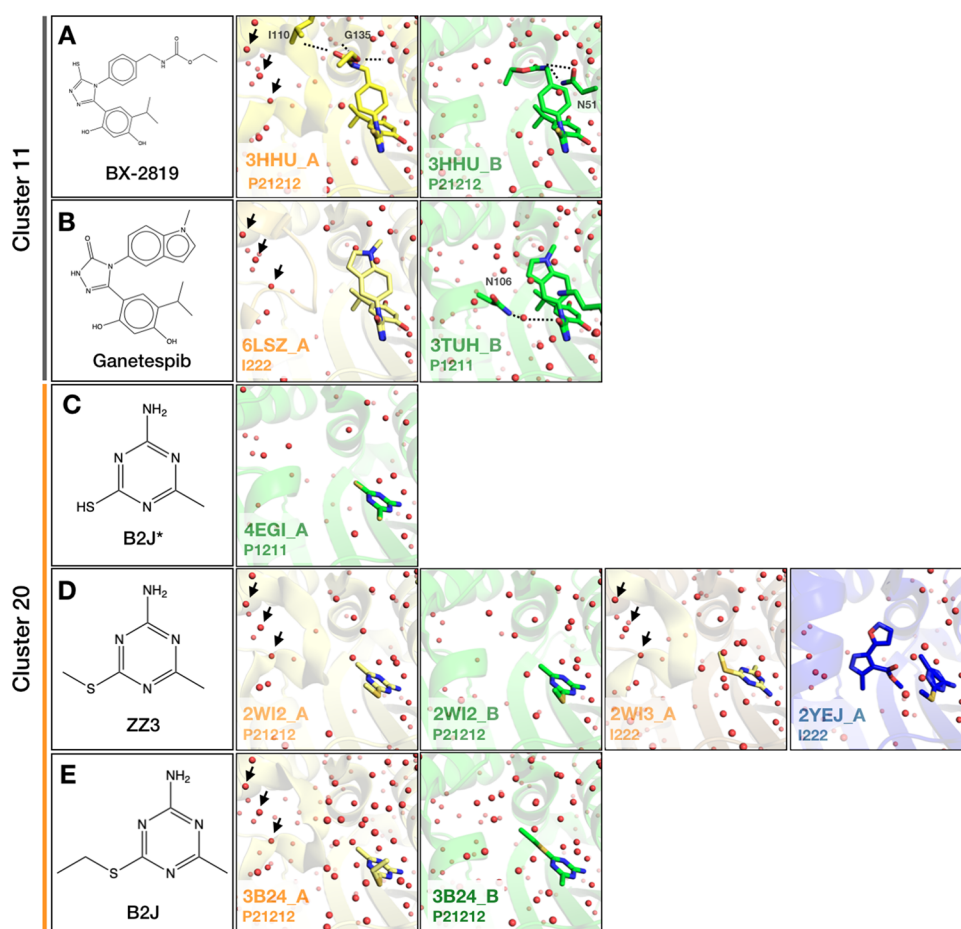
Figure 5. Related ligands change poses and loop conformations. (A) BX-2819 bound to Hsp90α-NTD in 3HHU has a different pose and hydrogen bonds (dotted lines) when bound to the loop-in state in chain A and the loop-out state in chain B, shown in center and right panels, respectively. (B) Closely related ganetespib (Tc ≈ 0.7) bound to loop-in and loop-out conformations in separate structures and adopted a similar pose; shown in center and right panels, respectively. Arrows indicate waters present in the "loop in" conformation that are displaced in the "loop out" conformation, and vice versa. (C−E) Poses of related fragments in cluster 20 change with lid conformation and fragment size. (C) B2J was crystallized in 4EGI but electron density for the ethyl tail is missing. The truncated fragment, here called B2J*, was modeled in two poses with the sulfur atom on either side of the triazine ring. (D) ZZ3 contains an additional methyl on the sulfur as it is bound to both loop-in and loop-out states with the same pose within the same crystal structure but bound in a different pose in the loop-in state of a separate crystal structure. Crystallization with a second fragment in 2YEJ causes a change in both the pose and lid state. (E) B2J contains an ethyl tail on the sulfur atom and is seen in the same pose as ZZ3 when bound to the loop-in state but a different pose when bound to the loop-out state.

ligand set occupied discrete regions of the binding site, especially along the lid (Figure 2B). To further interrogate the relation between ligand accessibility and lid conformation, we created binary protein−ligand "fingerprints" based on whether each residue in the structure was near ($\leq$5 Å) or far (>5 Å) from a particular ligand. Hierarchical clustering of these fingerprints based on Tanimoto similarity (Tc) confirmed that protein−ligand interactions are generally distinguishable by lid conformation (Figure 2C; for exceptions, see SI, Figure S8).

Conformation-Specific Ligands Exhibit Distinct Chemical Properties. Our observations of conformation-specific hotspots suggested that the chemical properties of ligands differ with their binding-site shapes. To explore the relations between ligand properties and major lid conformations, we exploited the chemical diversity (238 unique ligands, 298 total) in the investigated dataset that contains fragments, leads, and drug-like molecules. As the binding-site volume increased, so did the ligand size: the loop-in binders were smaller than the loop-out binders, and both were smaller than the helical binders (Figure 3A; $p < 0.05$). The topological polar

surface area (tPSA) was also greater for ligands binding the helical and loop-out conformations than for those binding the loop-in state (Figure 3B; $p < 0.05$). The lipophilicity partition coefficient (aLogP) of helical binders was higher than that of the two loop states (Figure 3C; $p < 0.05$). Plotting aLogP against molecular weight (MW) highlighted how dissimilar native substrates like ATP and its analogues are from most other binders (Figure 3D). Median IC_{50} values indicated that molecules with the highest affinity tend to bind the helical state rather than either loop state (Figure 3E). Although this finding supports previous reports that linked the effect to the increased conformational flexibility of the helix compared to the loop state,[54] the IC_{50} distributions were broad, and the differences were not statistically significant. Although helical binders were, on average, much larger than loop binders, drug-like ligands bound all lid conformations with similar affinity (Figure 3F). However, many helical binders had affinities on par with fragments binding the loop states. The trend of smaller molecules having more ligand efficiency (LE),[65] which is measured as binding energy per ligand atom,[66] held true here:

larger ligands binding the helical conformation were less efficient than smaller ones binding the loop-in state (Figure 3A,G; $p < 0.05$). Again, tight binding did not necessarily imply lid preference, and weak ligands bound to all three states. Lipophilic efficiency (LipE) is a metric that combines affinity (IC_{50} values) with lipophilicity (aLogP) to estimate drug-likeness.[67] The loop-out binders had the worst median LipE values (Figure 3H). The median LipE for larger helical binders was close to that of smaller loop-in binders. Helical binders tended to vary in LipE and had similar LE values, and loop-in binders showed the opposite trend. Loop-out binders varied in both LipE and LE values (SI, Figure S9). Together, these results indicate that ligands that bind each lid conformation have distinguishable chemical properties.

Related Ligands Can Stabilize Different Loop Conformations and Change Poses. Small ligand changes can modify the binding landscape[36] and lead to different binding modes.[68] To explore whether related ligands can bind across the major lid states, we compared all pairwise ligand Tc similarities. This produced a bimodal distribution, suggesting the presence of at least two populations of related ligands (Figure 4A). Calculating separate pairwise Tc values based on their bound lid state produced three distinct populations (Figure 4A). Loop-in binders were less similar (median Tc = 0.21) than helical binders (median Tc = 0.40). Diversity did not increase with MW (Figure 3A), suggesting that helical binders include a series of related compounds created during hit optimization. For instance, 22 helical binders contained a purine scaffold.

To identify related ligands that bind different lid states, we employed hierarchical clustering. We used a Tc threshold of 0.6, based on the all-vs-all pairwise Tc values calculated in Figure 4A, to produce 108 clusters: 63 had more than one member, most of which contained fewer than 10 members (Figure 4B and SI, Figure S10 and Table S1). As expected, clusters of related ligands typically bound the same lid conformation, and some clusters again showed increased variability of the loop-out state. For instance, native Hsp90α ligands (e.g., ATP, ADP, and purine analogues) were closely related (Tc > 0.76) and clustered together (cluster 61) but bound a range of loop-out orientations (SI, Figure S11).

Two notable exceptions, which despite their high structural similarity (Tc = 0.7) bound different lid conformations, are BX-2819 and the clinical candidate ganetespib (Figure 5A,B and SI, Figure S12). We noticed that the BX-2819 complex crystallized in space group $P2_12_12$ and contained two copies in the asymmetric unit (ASU), while ganetespib crystallized in space group I222 or $P2_1$ with one or two copies in the ASU, respectively. Both the BX-2819 pose (RMSD 2.42 Å) and the lid conformation (RMSD 5.64 Å) differed considerably between chains. In chain A, BX-2819 formed an H-bond with Ile110 in the loop-in state; in chain B, it formed H-bonds with Asn51 on the opposite end of the loop-out binding site (Figure 5A). In contrast, ganetespib bound the lid in both loop states (lid RMSD 5.27 Å) with little change in ligand pose (ligand RMSD in chain A vs B: 0.48 Å) (Figure 5B and SI, Figure S12). The complexity of the relation between ligand binding and lid conformation was further emphasized by cluster 20 (Figure 5C−E and SI, Figure S13). Here, the smallest fragment in the series bound the loop-out conformation in two different poses (Figure 5C). With one added methyl group, fragment ZZ3 bound in the same pose in both chains within the same crystal structure but stabilized two

different lid conformations (loop-in and loop-out) (Figure 5D). Confusingly, the same ligand was observed in a different pose bound to the loop-in conformation in a separate structure (Figure 5D). In the presence of a second fragment, ZZ3 changed both the ligand pose and lid conformation (Figure 5D). When adding another methyl group to ZZ3, the ligand pose switched from the loop-in to the loop-out conformation (Figure 5E). Finally, we noted that lid changes perturbed binding-site water networks in otherwise identical protein−ligand complexes[6] (Figure 5).

Crystal Packing Affects Lid Preference and Vice Versa. Based on the observation of different ligand poses and lid conformations within the same crystal structure (Figure 5), we explored the connection between crystal packing and lid preference. We calculated the frequency of lid-specific structures for each space group. Remarkably, only the most frequently occurring space group, I222, contained structures with all three lid conformations (Figure 6A). The space group
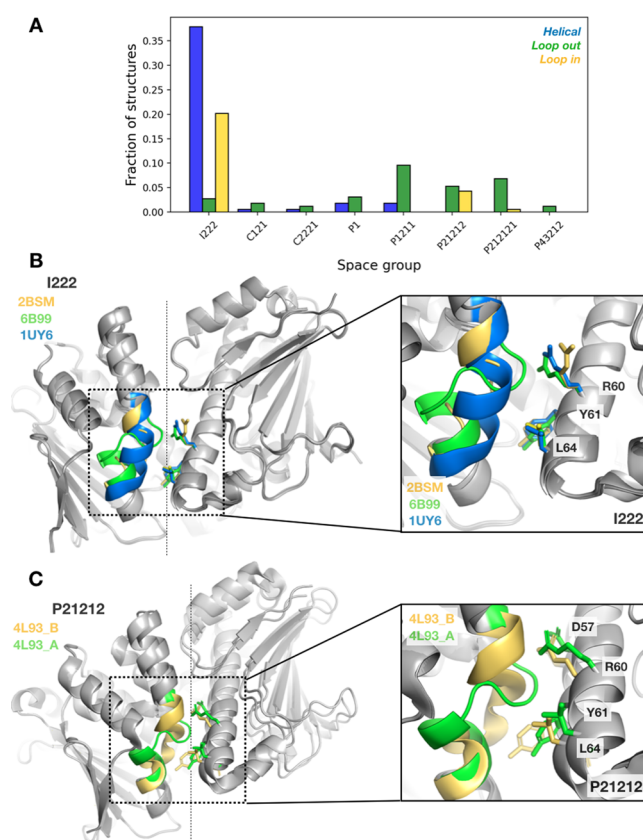

Figure 6. Crystal packing affects lid conformation preference and vice versa. (A) Frequency of lid conformations solved in each space group; see Table S2 for apo space groups. (B, C) Ribbon diagrams of representative structures of each lid state solved in I222 (B) and $P2_12_12$ (C).

of the BX-2819 complex, $P2_12_12$, contained only structures with loop-in or loop-out conformations in almost even proportions when we considered each chain separately. Notably, 6 of 14 $P2_12_12$ structures had one apo chain and one holo chain in the ASU. "Genuine" apo structures also crystallized in the $P2_1$ and I222 space groups (SI, Table S2). For the $P2_12_12$ structures in which the ligand was modeled in both chains, the ligand's pose often differed with the lid conformation (SI, Figure S14). These results indicate that

crystal packing in certain space groups restricted either binding and lid motion or packing preferences of liganded lid states.

A contact analysis of the respective lid state in each space group suggested that the lid was less restrained in I222, which has a single copy in the ASU, than in $P2_12_12$, which has two copies in the ASU. Sidechains of residues along the symmetry mate closest to the lid appeared to be flexible enough to accommodate shifts between loop conformations, hence enabling all three lid states to be populated in I222 (Figure 6B). In contrast, the ASU interface in $P2_12_12$ differed in the shift of the backbone helix (Figure 6C). The shift of this backbone, which is not present in I222, may prevent repositioning of the neighboring lid. These results stress that crystal packing can have a substantial but unappreciated impact on using structural data in ligand discovery and design efforts.

Molecular Docking Recapitulates Discrete Chemotypes across Lid States. To explore whether our categorization of lid states is meaningful for ligand discovery and recapitulates state-specific ligand properties, we conducted a retrospective docking study. We compared the docking performance of 88 known active binders and 7698 property-matched decoys[69] docked against a total of 12 lid conformations, using three models from each state as replicates (cf. Materials and Methods). All conformations showed similar enrichment; the loop-out models had the best overall enrichment (AUC: 0.77 ± 0.03) and early enrichment (logAUC: 0.22 ± 0.01) on average (Figure 7A and SI, Figure S15). This is also supported by enrichment factors, EF1 and EF2 (Figure S16). However, the top 500 scoring compounds differed between lid conformations; each state contributed at least 271 and as many as 392 new compounds to the top 500 (Figure 7B,C). The Tc similarity of molecules was higher within loop states and helical states (i.e., helical and minor) than across states (Figure 7B). Considering the relatively small number of docked compounds and similarity of conformations, only few of the top 500 compounds were shared (Figure 7C). This finding highlights that docking to each state produced compounds with distinct chemotypes. Although the data are sparse, this is also true when considering only active molecules in the top 500 docked compounds (Figure S18). Also, the observed relations across ligand properties (i.e., MW, aLogP, and tPSA) and lid conformation followed similar trends (SI, Figure S17) as the crystallographic data (Figure 3). Again, ligand diversity decreased as lid-defined binding site volumes and ligand sizes increased (Figure 7D and SI, Figure 17A). Using pose recapitulation as a metric for docking performance of each lid state, we found that "helical" receptors produced the best matching poses in 10 of 14 crystal structures (Figure 7E and SI, Figure S19 and Table S3). In four of 14 cases, the docked pose and receptor lid conformation matched the crystallographic model. Conceivably, for ligands where the best docked pose preferred a lid conformation different than the crystal structure, binding often does not involve interactions with the lid. Two notable helical binders were the purine-based inhibitor PU1 and the clinical candidate BIIB021 (94M)[70] (Figure 7F,G). In both cases, loop models poorly reproduced crystal structure poses. Meanwhile, the helical states to which these molecules bound correctly predicted the crystal poses (0.38 Å for 94M and 1.47 Å for PU1). The success of docking 94M to the minor conformation highlighted the utility of this state as an alternative to the helical model. These docking results reinforce the notion that state-specific ligands exhibit distinct chemical properties and capitalize on subtle but
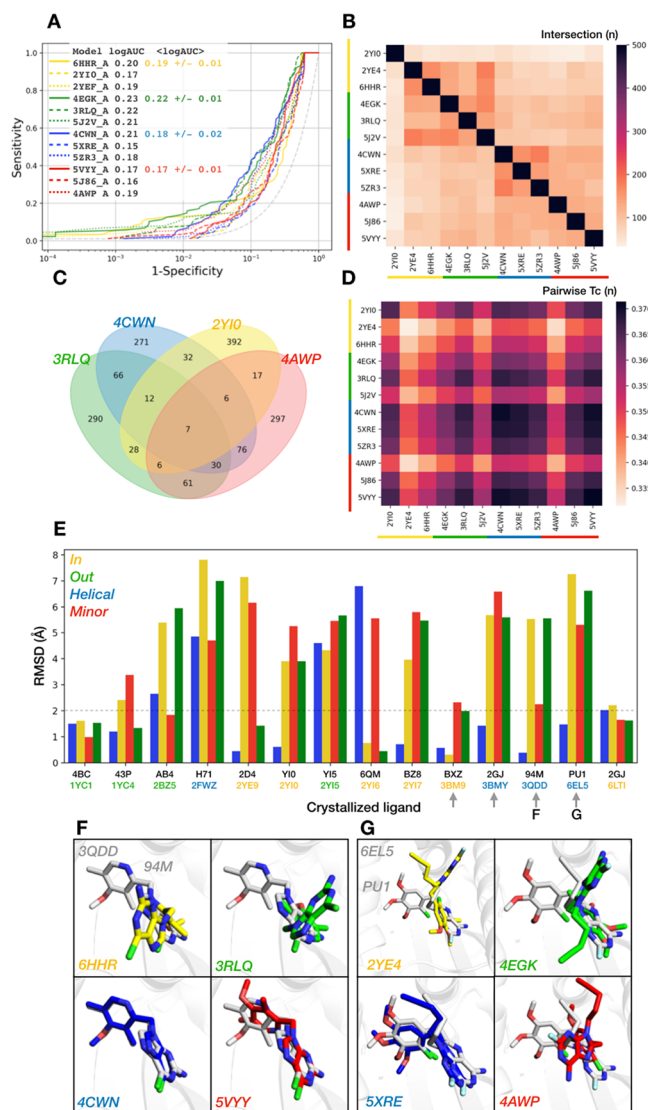

Figure 7. Docking against major and minor lid states recapitulates distinct chemotypes. (A) Semilogarithmic ROC curves for 12 models (three for each conformation) used for retrospective docking to Hsp90α DUDE-E subset.[69] The plot legend shows logAUC values for each PDB model and average logAUC values for each conformation. (B) Pairwise comparison of the top 500 shared molecules for each model. (C) Venn diagram of the top 500 shared molecules across models with the best AUC value for each conformation. (D) Pairwise Tanimoto coefficients (Tc) for the top 500 molecules. (E) RMSD values calculated between the docked pose and crystallographic pose for models with the lowest RMSD value within each conformation. Arrows indicate that the best docked-pose matches with crystallographic lid conformation. Two examples are shown in (F) for 94M bound to 3QDD (gray) and (G) for PU1 bound to 6EL5 (gray). RMSD values for all models are shown in SI, Figure S19 and Table S3. Colors throughout refer to the lid conformation (yellow; loop-in, green: loop-out, blue: helical, and red: minor).

meaningful conformational differences. In turn, while the field struggles to find molecules that distinguish sequence-similar isoforms, this systematic ensemble approach has shown that unique chemotypes can stabilize distinct states, even within a single isoform.

■ DISCUSSION

This study highlights the utility of using ligands to perturb the protein conformational landscape with a view toward ligand discovery. In the absence of explicit dynamic data, a rich dataset of over 300 ligand-perturbed structures afforded new insights into state-specific, targetable hotspots. Three main implications for ligand discovery emerged from this work: First, three major and three minor Hsp90α lid conformations provide distinct structural templates to find state-specific ligands. Second, ligands with distinguishable chemical properties generally complement specific lid states with insightful exceptions; docking recapitulates state-specific chemotype differences. Third, crystal packing affects lid preference and vice versa, which influences medicinal chemistry decisions.

Perplexed by the large number of possible Hsp90α structural templates and without reliable energy weighting,[71] ligand discoverers typically resort to focusing on two conformations and a few ligands. Our study differed from this minimalist approach in that it systematically broke down the complexity of ligandable Hsp90α conformational space into three major and three minor targetable conformations. This reflects the sentiment that everything should be made as simple as possible but no simpler. For instance, loop-in and loop-out states are typically treated as a single loop conformation,[54] but as we show here, these states have considerably different binding-site surfaces. Focusing on a handful of states that represents vital areas of Hsp90's conformational landscape, instead of hundreds of structures, enables us to consider all representative states simultaneously without unreasonably compromising computational speed. For instance, we previously applied a Boltzmann-weighted flexible-docking approach on another system to find chemically novel ligands against a total of 16 states with only a 2.4-fold slowdown compared to using a single template.[9] If we consider a Boltzmann distribution, the three major loop states would require lower energy payments for ligand binding than the less-frequented minor states. Of the major states, the loop-in conformation appears lowest in energy as it is the dominant state within apo structures and ligands pay a smaller energetic penalty to stabilize this state. The helical state is not present in apo structures, but it is the most populated one among holo structures. Helical binders are significantly larger and among the tightest binders due to increased flexibility of the lid helix.[54] As we showed here, helical binders often add more bulk and reduce ligand efficiency, but their overall beneficial thermodynamic and kinetic contributions to binding[54] outweigh the conformational penalties. This justifies targeting this state later in the drug-discovery process to achieve toxicity-mitigating isoform selectivity,[72] though most early-stage fragments may not be able to pay the protein conformational penalty and instead bind one of the loop states. Along the same lines, targeting high-energy minor states, such as those identified in this study, can provide novel opportunities to stabilize rare Hsp90 conformations. Those lid states not only create unique hotspots for ligand binding but also have been shown to engage other proteins involved in driving the Hsp90 conformational cycle. Alternative lid conformations may change interaction patterns with clients, co-chaperones, and post-translational modifiers[42,45,73] and result in new biology as those interactions differ among isoforms.

Medicinal chemistry pragmatism assumes that small ligand modifications do not result in large protein changes. Although this assumption generally holds true here, as ligand chemistry correlates with lid preference, congeneric ligand series also stabilize different conformational states.[74] During drug design, a growing ligand may push the lid into a new state and possibly lose affinity as penalties differ between states. These exceptions are a nuisance for prospective ligand optimization; however, they provide insights to improve retrospective ligand discovery. For instance, consider a case in which the protein transitions from the loop-in to the helical state upon binding two near-identical ligands. Docking to a single state would capture one ligand but not its analogue; an ensemble approach will cover both. Prominent examples of ligands with unfulfilled clinical potential are the closely related molecules BX-2819 and ganetespib,[75,76] both of which showed crystal structure flexibility of the ligand and protein, which allows for at least two binding modes.

Further compounding the problem, we found examples of identical ligands binding across lid states with or without changing poses. First, from a ligand perspective, docking success is measured by agreement between the predicted and experimental ligand pose. From a protein perspective, different input structures will significantly change docking performance.[2,71] As each lid state contributes more than half of the top 500 compounds that differ in chemotype across states, an ensemble approach can help overcome some limitations of traditional docking.[77,78] Second, both ligand and protein changes will change the binding-site water networks.[79,80] Penalties for displacing or retaining waters significantly contribute to ligand binding[6,81,82] and can mediate isoform selectivity.[83,84] Current estimates of entropic differences of lid states have identified conserved water clusters by using crystallography and molecular dynamics but do not differentiate between the two loop states that show clear differences in water structure in our analysis.[54] Due to the important role of water in Hsp90,[54,85−88] careful consideration of water networks in both the ground state and relevant bound states determines the thermodynamic binding signatures and desolvation penalties[79,89] that will guide ligand discovery and design.[90−92] Notably, recent work on Hsp90 demonstrates that water networks repopulate protein-ligand binding sites with temperature,[93] which can impact docking performance metrics like enrichment.[2]

Finally, the use of state-dependent energy penalties assumes minimal experimental artifacts. However, our analysis suggested a relation between space group and lid preference. Although co-crystallization would imply that lid conformations stabilize crystal packing, soaking would raise concerns that pre-packed crystals restrict lid mobility to accommodate ligands and may explain some of the curious cases observed here. Pose changes of fragments upon soaking vs co-crystallization have been previously observed for Hsp90[94] and protein kinase A.[95] While the lack of consistent reporting prohibits us from disentangling cause and effect, packing artifacts that distort the protein conformational landscape also impede our ability to rationally explore the landscape's features during ligand discovery.[77] For flexible proteins with induced protein adaptations to ligand binding, co-crystallization is recommended because it more faithfully recapitulates protein−ligand interactions. Soaking differences amplify with ligand size and flexibility.[95] Considering this underappreciated aspect may avoid medicinal chemistry detours that involuntarily optimize crystal packing rather than ligand binding for Hsp90 space groups other than I222.

Another caveat that merits discussion is that breaking down 321 structural states into six distinct clusters by no means indicates that the Hsp90α conformational landscape is simpler than anticipated. The conformational heterogeneity we observed for the loop-out state illustrated that complexity is infinitely tunable. For instance, if exclusive targeting of the loop-out state is desired, one may consider an ensemble treatment of all its 103 substates to achieve more granularity of conformational space. Indeed, the apo-absent helical conformation and the presence of minor helical states further illuminated promising avenues for exploiting protein flexibility and forcing new conformations to improve selectivity or affinity.[68] We note that this approach will work best for flexible proteins with sufficient representation in the PDB. Our survey suggest that 393 unique proteins have 50 or more structures in the PDB, of which 143 have over 100 structural representatives (Figure S20).

In summary, ligands provide a means to perturb the protein conformational landscape and stabilize distinct populations from a dynamic ensemble of conformational states. The availability of over 300 ligand-perturbed Hsp90α structures enabled a data-driven approach to determine how ligands with distinguishable properties are accommodated in a dynamic binding site. For Hsp90 (mal)function, this is of note as chemotype-dependent binding conformations appear to strongly influence isoform[48,72,96] and species selectivity.[97] Besides lid preferences and hotspots, our ligand perturbation approach also revealed some unappreciated caveats of current drug-discovery campaigns. As these caveats are not specific to this protein, the results inform a generalizable ensemble-based approach to ligand discovery against dynamic proteins using a large set of individual static snapshots.

MATERIALS AND METHODS

The coordinates for 312 Hps90α-NTD structures were downloaded from the PDB.[53] Individual chains were considered as separate structures in the analysis and extracted with the "split_chains" function in PyMOL. The RSCC values were computed using the Phenix program "phenix.real_space_correlation".[98] Convex hulls and volumes were calculated using the "convexhull" function from the SciPy Python library (v1.5.0) and the coordinates of Cα atoms in residues Asn51, Ser52, Ala55, Asp93, Ile96, Gly97, Met98, Leu103, Leu107, Thr109, Phe138, Tyr139, Val150, Trp162, Thr184, and Val186. Ligand-binding hotspots were created with a custom Python (v3.8.3) script by calculating how often each residue (any non-H atom) was within 5 Å of ligands (any non-H atom). Similarly, binary protein−ligand fingerprints were created by assigning 0's to residues >5 Å away from any non-H ligand atom and 1's for residues with distances of ≤5 Å. Hierarchical clustering of these fingerprints was performed with the "hierarchy" function from the SciPy Python library (v.1.7.1) by using the Jaccard distance metric and single-linkage method. The probability-distribution function of ligand position was computed using the aligned ligand coordinates and the "PDF" function in Mathematica. Atomic space-filling was approximated by randomly generating a number of points proportional to the atomic number within the covalent radius of each atom. The chemical properties of ligands and fingerprints were computed using RDKit (v2021.09.4) in Python (v3.9.4). For docking, 88 actives and 7698 decoys were taken from the Hsp90 DUDE-E subset.[69] Protein structures were selected for docking by taking the centroid structure of each distribution, i.e., with the median binding-site volume, plus the two structures immediately adjacent to the median for each conformation; all other differences were ignored. Molecules were docked using Glide (Schrödinger) with Standard Precision (SP) and default settings.[99] Hierarchical clustering based on ligand similarity was performed as above. IC_{50} values were obtained from the PDB,

and the lowest value was used in the analysis if multiple IC_{50} values were reported for a particular ligand.

ASSOCIATED CONTENT

Supporting Information

The Supporting Information is available free of charge at https://pubs.acs.org/doi/10.1021/acs.jmedchem.2c00708.

Quality assessment Hsp90α-NTD models; diagrams of the structures classified by each lid conformation; mean deviation calculations of Hsp90α-NTD; plots of pairwise difference mean deviation values based on lid classification; electron density maps of the lid in small-volume outliers; diagrams of the minor helical states; histogram showing the frequency of residues near ligands based on lid conformation; examples of ligands with similar protein−ligand fingerprints but different lid conformations when sulfate is bound; relationships of lipophilic efficiency and ligand efficiency with lid conformation; chemical structures of the cluster centroids; diagram of cluster 58 ligands; comparison of ganetespib poses between chains; RMSD heat map of proteins with ligands in cluster 20; comparison of ligand and protein RMSD in P2₁2₁2 structures; docking ROC curve with AUC values; chemical properties of the top 500 docked compounds; RMSD values of pose reproduction; table of cluster members; table of apo space groups; table of RMSD values for pose reproduction (PDF)

AUTHOR INFORMATION

Corresponding Author

Marcus Fischer − *Department of Chemical Biology & Therapeutics and Department of Structural Biology, St. Jude Children's Research Hospital, Memphis, Tennessee 38105, United States;* orcid.org/0000-0002-7179-2581; Phone: (901)-595-6269; Email: marcus.fischer@stjude.org

Author

Timothy R. Stachowski − *Department of Chemical Biology & Therapeutics, St. Jude Children's Research Hospital, Memphis, Tennessee 38105, United States*

Complete contact information is available at:
https://pubs.acs.org/10.1021/acs.jmedchem.2c00708

Author Contributions

T.R.S. and M.F. designed the research; T.R.S. performed the research and contributed new reagents/analytic tools; T.R.S. and M.F. analyzed the data and wrote the paper.

Notes

The authors declare no competing financial interest.

ACKNOWLEDGMENTS

ABBREVIATIONS

Cα, alpha carbon; ASU, asymmetric unit; Hsp90, heat shock protein 90; Hsp90α, heat shock protein 90-alpha; LipE, lipophilic efficiency; MDev, mean deviation; NTD, N-terminal domain; RSCC, real space correlation coefficient; ROC, receiver operating characteristic; Tc, Tanimoto similarity; tPSA, topological polar surface area

REFERENCES

(1) Copeland, R. A. Conformational adaptation in drug-target interactions and residence time. *Future Med. Chem.* **2011**, *3*, 1491−1501.

(2) Bradford, S.; Khoury, L.; Ge, Y.; Osato, M.; Mobley, D.; Fischer, M. Temperature artifacts in protein structures bias ligand-binding predictions. *Chem. Sci.* **2021**, *12*, 11275−11293.

(3) Spyrakis, F.; BidonChanal, A.; Barril, X.; Luque, F. J. Protein flexibility and ligand recognition: Challenges for molecular modeling. *Curr. Top. Med. Chem.* **2011**, *11*, 192−210.

(4) Stank, A.; Kokh, D. B.; Fuller, J. C.; Wade, R. C. Protein binding pocket dynamics. *Acc. Chem. Res.* **2016**, *49*, 809−815.

(5) Boehr, D. D.; Nussinov, R.; Wright, P. E. The role of dynamic conformational ensembles in biomolecular recognition. *Nat. Chem. Biol.* **2009**, *5*, 789−796.

(6) Darby, J. F.; Hopkins, A. P.; Shimizu, S.; Roberts, S. M.; Brannigan, J. A.; Turkenburg, J. P.; Thomas, G. H.; Hubbard, R. E.; Fischer, M. Water networks can determine the affinity of ligand binding to proteins. *J. Am. Chem. Soc.* **2019**, *141*, 15818−15826.

(7) Di Cera, E. Mechanisms of ligand binding. *Biophys. Rev.* **2020**, *1*, No. 011303.

(8) Vogt, A. D.; Pozzi, N.; Chen, Z.; Di Cera, E. Essential role of conformational selection in ligand binding. *Biophys. Chem.* **2014**, *186*, 13−21.

(9) Fischer, M.; Coleman, R. G.; Fraser, J. S.; Shoichet, B. K. Incorporation of protein flexibility and conformational energy penalties in docking screens to improve ligand discovery. *Nat. Chem.* **2014**, *6*, 575−583.

(10) Fernández-Quintero, M. L.; Pomarici, N. D.; Loeffler, J. R.; Seidler, C. A.; Liedl, K. R. T-cell receptor CDR3 loop conformations in solution shift the relative Vα-Vβ domain distributions. *Front. Immunol.* **2020**, *11*, 1440.

(11) Koshland, D. E. Enzyme flexibility and enzyme action. *J. Cell Comp. Physiol.* **1959**, *54*, 245−258.

(12) Changeux, J. P. Allostery and the Monod-Wyman-Changeux model after 50 years. *Annu. Rev. Biophys.* **2012**, *41*, 103−133.

(13) Cui, Q.; Karplus, M. Allostery and cooperativity revisited. *Protein Sci.* **2008**, *17*, 1295−1307.

(14) Hammes, G. G.; Chang, Y. C.; Oas, T. G. Conformational selection or induced fit: A flux description of reaction mechanism. *Proc. Natl. Acad. Sci. U. S. A.* **2009**, *106*, 13737−13741.

(15) Vega, S.; Abian, O.; Velazquez-Campoy, A. On the link between conformational changes, ligand binding and heat capacity. *Biochim. Biophys. Acta* **2016**, *1860*, 868−878.

(16) Miller, M. D.; Phillips, G. N. Moving beyond static snapshots: Protein dynamics and the protein data bank. *J. Biol. Chem.* **2021**, *296*, 100749.

(17) Henzler-Wildman, K.; Kern, D. Dynamic personalities of proteins. *Nature* **2007**, *450*, 964−972.

(18) Austin, R. H.; Beeson, K. W.; Eisenstein, L.; Frauenfelder, H.; Gunsalus, I. C. Dynamics of ligand binding to myoglobin. *Biochemistry* **1975**, *14*, 5355−5373.

(19) Frauenfelder, H.; Sligar, S. G.; Wolynes, P. G. The energy landscapes and motions of proteins. *Science* **1991**, *254*, 1598−1603.

(20) Zimmerman, M. I.; Porter, J. R.; Ward, M. D.; Singh, S.; Vithani, N.; Meller, A.; Mallimadugula, U. L.; Kuhn, C. E.; Borowsky, J. H.; Wiewiora, R. P.; Hurley, M. F. D.; Harbison, A. M.; Fogarty, C. A.; Coffland, J. E.; Fadda, E.; Voelz, V. A.; Chodera, J. D.; Bowman, G. R. SARS-CoV-2 simulations go exascale to predict dramatic spike opening and cryptic pockets across the proteome. *Nat. Chem.* **2021**, *13*, 651−659.

(21) Fischer, M.; Shoichet, B. K.; Fraser, J. S. One crystal, two temperatures: Cryocooling penalties alter ligand binding to transient protein sites. *ChemBioChem* **2015**, *16*, 1560−1564.

(22) Lerner, E.; Barth, A.; Hendrix, J.; Ambrose, B.; Birkedal, V.; Blanchard, S. C.; Börner, R.; Sung Chung, H.; Cordes, T.; Craggs, T. D.; Deniz, A. A.; Diao, J.; Fei, J.; Gonzalez, R. L.; Gopich, I. V.; Ha, T.; Hanke, C. A.; Haran, G.; Hatzakis, N. S.; Hohng, S.; Hong, S. C.; Hugel, T.; Ingargiola, A.; Joo, C.; Kapanidis, A. N.; Kim, H. D.; Laurence, T.; Lee, N. K.; Lee, T. H.; Lemke, E. A.; Margeat, E.; Michaelis, J.; Michalet, X.; Myong, S.; Nettels, D.; Peulen, T. O.; Ploetz, E.; Razvag, Y.; Robb, N. C.; Schuler, B.; Soleimaninejad, H.; Tang, C.; Vafabakhsh, R.; Lamb, D. C.; Seidel, C. A.; Weiss, S. FRET-based dynamic structural biology: Challenges, perspectives and an appeal for open-science practices. *Elife* **2021**, *10*, e60416.

(23) Lento, C.; Wilson, D. J. Subsecond time-resolved mass spectrometry in dynamic structural biology. *Chem. Rev.* **2022**, *122*, 7624−7646.

(24) Henzler-Wildman, K. A.; Lei, M.; Thai, V.; Kerns, S. J.; Karplus, M.; Kern, D. A hierarchy of timescales in protein dynamics is linked to enzyme catalysis. *Nature* **2007**, *450*, 913−916.

(25) Putnam, C. D.; Hammel, M.; Hura, G. L.; Tainer, J. A. X-ray solution scattering (SAXS) combined with crystallography and computation: Defining accurate macromolecular structures, conformations and assemblies in solution. *Q. Rev. Biophys.* **2007**, *40*, 191−285.

(26) Robertson, M. J.; Meyerowitz, J. G.; Skiniotis, G. Drug discovery in the era of cryo-electron microscopy. *Trends Biochem. Sci.* **2022**, *47*, 124−135.

(27) Chapman, H. N. X-ray free-electron lasers for the structure and dynamics of macromolecules. *Annu. Rev. Biochem.* **2019**, *88*, 35−58.

(28) Keedy, D. A. Journey to the center of the protein: Allostery from multitemperature multiconformer x-ray crystallography. *Acta Crystallogr., Sect. D: Struct. Biol.* **2019**, *75*, 123−137.

(29) Fischer, M. Macromolecular room temperature crystallography. *Q. Rev. Biophys.* **2021**, *54*, No. e1.

(30) Socher, E.; Sticht, H. Mimicking titration experiments with md simulations: A protocol for the investigation of pH-dependent effects on proteins. *Sci. Rep.* **2016**, *6*, 22523.

(31) Yang, F.; Phillips, G. N., Jr. Crystal structures of co-, deoxy- and met-myoglobins at various ph values. *J. Mol. Biol.* **1996**, *256*, 762−774.

(32) Sanchez-Weatherby, J.; Bowler, M. W.; Huet, J.; Gobbo, A.; Felisaz, F.; Lavault, B.; Moya, R.; Kadlec, J.; Ravelli, R. B.; Cipriani, F. Improving diffraction by humidity control: A novel device compatible with x-ray beamlines. *Acta Crystallogr., Sect. D: Struct. Biol.* **2009**, *65*, 1237−1246.

(33) Douangamath, A.; Aller, P.; Lukacik, P.; Sanchez-Weatherby, J.; Moraes, I.; Brandao-Neto, J. Using high-throughput in situ plate screening to evaluate the effect of dehydration on protein crystals. *Acta Crystallogr., Sect. D: Struct. Biol.* **2013**, *69*, 920−923.

(34) Hekstra, D. R.; White, K. I.; Socolich, M. A.; Henning, R. W.; Šrajer, V.; Ranganathan, R. Electric-field-stimulated protein mechanics. *Nature* **2016**, *540*, 400−405.

(35) Collins, M. D.; Kim, C. U.; Gruner, S. M. High-pressure protein crystallography and NMR to explore protein conformations. *Annu. Rev. Biophys.* **2011**, *40*, 81−98.

(36) Mobley, D. L.; Dill, K. A. Binding of small-molecule ligands to proteins: "What you see" is not always "what you get". *Structure* **2009**, *17*, 489−498.

(37) Ma, B.; Kumar, S.; Tsai, C. J.; Nussinov, R. Folding funnels and binding mechanisms. *Protein Eng.* **1999**, *12*, 713−720.

(38) Gutteridge, A.; Thornton, J. M. Understanding nature's catalytic toolkit. *Trends Biochem. Sci.* **2005**, *30*, 622−629.

(39) Trepel, J.; Mollapour, M.; Giaccone, G.; Neckers, L. Targeting the dynamic Hsp90 complex in cancer. *Nat. Rev. Cancer* **2010**, *10*, 537−549.

(40) Whitesell, L.; Lindquist, S. L. Hsp90 and the chaperoning of cancer. *Nat. Rev. Cancer* **2005**, *5*, 761−772.

(41) Garg, G.; Khandelwal, A.; Blagg, B. S. Anticancer inhibitors of Hsp90 function: Beyond the usual suspects. *Adv. Cancer Res.* **2016**, *129*, 51−88.

(42) Schopf, F. H.; Biebl, M. M.; Buchner, J. The Hsp90 chaperone machinery. *Nat. Rev. Mol. Cell Biol.* **2017**, *18*, 345−360.

(43) Krukenberg, K. A.; Street, T. O.; Lavery, L. A.; Agard, D. A. Conformational dynamics of the molecular chaperone Hsp90. *Q. Rev. Biophys.* **2011**, *44*, 229−255.

(44) Prodromou, C.; Roe, S. M.; O'Brien, R.; Ladbury, J. E.; Piper, P. W.; Pearl, L. H. Identification and structural characterization of the ATP/ADP-binding site in the Hsp90 molecular chaperone. *Cell* **1997**, *90*, 65−75.

(45) Colombo, G.; Morra, G.; Meli, M.; Verkhivker, G. Understanding ligand-based modulation of the Hsp90 molecular chaperone dynamics at atomic resolution. *Proc. Natl. Acad. Sci. U. S. A.* **2008**, *105*, 7976−7981.

(46) Stebbins, C. E.; Russo, A. A.; Schneider, C.; Rosen, N.; Hartl, F. U.; Pavletich, N. P. Crystal structure of an Hsp90-geldanamycin complex: Targeting of a protein chaperone by an antitumor agent. *Cell* **1997**, *89*, 239−250.

(47) Li, J.; Sun, L.; Xu, C.; Yu, F.; Zhou, H.; Zhao, Y.; Zhang, J.; Cai, J.; Mao, C.; Tang, L.; Xu, Y.; He, J. Structure insights into mechanisms of ATP hydrolysis and the activation of human heat-shock protein 90. *Acta Biochim. Biophys. Sin.* **2012**, *44*, 300−306.

(48) Ernst, J. T.; Liu, M.; Zuccola, H.; Neubert, T.; Beaumont, K.; Turnbull, A.; Kallel, A.; Vought, B.; Stamos, D. Correlation between chemotype-dependent binding conformations of Hsp90α/β and isoform selectivity-implications for the structure-based design of Hsp90α/β selective inhibitors for treating neurodegenerative diseases. *Bioorg. Med. Chem. Lett.* **2014**, *24*, 204−208.

(49) Wright, L.; Barril, X.; Dymock, B.; Sheridan, L.; Surgenor, A.; Beswick, M.; Drysdale, M.; Collier, A.; Massey, A.; Davies, N.; Fink, A.; Fromont, C.; Aherne, W.; Boxall, K.; Sharp, S.; Workman, P.; Hubbard, R. E. Structure-activity relationships in purine-based inhibitor binding to Hsp90 isoforms. *Chem. Biol.* **2004**, *11*, 775−785.

(50) Ernst, J. T.; Neubert, T.; Liu, M.; Sperry, S.; Zuccola, H.; Turnbull, A.; Fleck, B.; Kargo, W.; Woody, L.; Chiang, P.; Tran, D.; Chen, W.; Snyder, P.; Alcacio, T.; Nezami, A.; Reynolds, J.; Alvi, K.; Goulet, L.; Stamos, D. Identification of novel Hsp90alpha/beta isoform selective inhibitors using structure-based drug design. Demonstration of potential utility in treating CNS disorders such as Huntington's disease. *J. Med. Chem.* **2014**, *57*, 3382−3400.

(51) Brough, P. A.; Aherne, W.; Barril, X.; Borgognoni, J.; Boxall, K.; Cansfield, J. E.; Cheung, K. M.; Collins, I.; Davies, N. G.; Drysdale, M. J.; Dymock, B.; Eccles, S. A.; Finch, H.; Fink, A.; Hayes, A.; Howes, R.; Hubbard, R. E.; James, K.; Jordan, A. M.; Lockie, A.; Martins, V.; Massey, A.; Matthews, T. P.; McDonald, E.; Northfield, C. J.; Pearl, L. H.; Prodromou, C.; Ray, S.; Raynaud, F. I.; Roughley, S. D.; Sharp, S. Y.; Surgenor, A.; Walmsley, D. L.; Webb, P.; Wood, M.; Workman, P.; Wright, L. 4,5-diarylisoxazole Hsp90 chaperone inhibitors: Potential therapeutic agents for the treatment of cancer. *J. Med. Chem.* **2008**, *51*, 196−218.

(52) Koren, J.; Blagg, B. S. J. The right tool for the job: An overview of Hsp90 inhibitors. *Adv. Exp. Med. Biol.* **2020**, *1243*, 135−146.

(53) Goodsell, D. S.; Zardecki, C.; Di Costanzo, L.; Duarte, J. M.; Hudson, B. P.; Persikova, I.; Segura, J.; Shao, C.; Voigt, M.; Westbrook, J. D.; Young, J. Y.; Burley, S. K. RCSB Protein Data Bank: Enabling biomedical research and drug discovery. *Protein Sci.* **2020**, *29*, 52−65.

(54) Amaral, M.; Kokh, D. B.; Bomke, J.; Wegener, A.; Buchstaller, H. P.; Eggenweiler, H. M.; Matias, P.; Sirrenberg, C.; Wade, R. C.; Frech, M. Protein conformational flexibility modulates kinetics and thermodynamics of drug binding. *Nat. Commun.* **2017**, *8*, 2276.

(55) Güldenhaupt, J.; Amaral, M.; Kötting, C.; Schartner, J.; Musil, D.; Frech, M.; Gerwert, K. Ligand-induced conformational changes in HSP90 monitored time resolved and label free-towards a conforma-

tional activity screening for drug discovery. *Angew. Chem., Int. Ed.* **2018**, *57*, 9955−9960.

(56) Morra, G.; Meli, M.; Colombo, G. How the ligand-induced reorganization of protein internal energies is coupled to conformational events. *J. Chem. Theory Comput.* **2018**, *14*, 5992−6001.

(57) Chen, J.; Wang, J.; Lai, F.; Wang, W.; Pang, L.; Zhu, W. Dynamics revelation of conformational changes and binding modes of heat shock protein 90 induced by inhibitor associations. *RSC Adv.* **2018**, *8*, 25456−25467.

(58) Yoshimura, C.; Nagatoishi, S.; Kuroda, D.; Kodama, Y.; Uno, T.; Kitade, M.; Chong-Takata, K.; Oshiumi, H.; Muraoka, H.; Yamashita, S.; Kawai, Y.; Ohkubo, S.; Tsumoto, K. Thermodynamic dissection of potency and selectivity of cytosolic Hsp90 inhibitors. *J. Med. Chem.* **2021**, *64*, 2669−2677.

(59) Wankowicz, S. A.; de Oliveira, S. H.; Hogan, D. W.; van den Bedem, H.; Fraser, J. S. Ligand binding remodels protein side chain conformational heterogeneity. *Elife* **2022**, *11*, No. e74114.

(60) Modi, V.; Dunbrack, R. L., Jr. Defining a new nomenclature for the structures of active and inactive kinases. *Proc. Natl. Acad. Sci. U. S. A.* **2019**, *116*, 6818−6827.

(61) Parker, M. I.; Meyer, J. E.; Golemis, E. A.; Dunbrack, R. L. Defining an expanded RAS conformational landscape based on over 700 experimentally determined structures of KRAS, NRAS, and HRAS. *bioRxiv* **2022**, DOI: 10.1101/2022.02.02.478568.

(62) Coleman, R. G.; Sharp, K. A. Protein pockets: Inventory, shape, and comparison. *J. Chem. Inf. Model.* **2010**, *50*, 589−603.

(63) Yabukarski, F.; Biel, J. T.; Pinney, M. M.; Doukov, T.; Powers, A. S.; Fraser, J. S.; Herschlag, D. Assessment of enzyme active site positioning and tests of catalytic mechanisms through x-ray-derived conformational ensembles. *Proc. Natl. Acad. Sci. U. S. A.* **2020**, *117*, 33204−33215.

(64) van den Noort, M.; de Boer, M.; Poolman, B. Stability of ligand-induced protein conformation influences affinity in maltose-binding protein. *J. Mol. Biol.* **2021**, *433*, 167036.

(65) Fischer, M.; Hubbard, R. E. Fragment-based ligand discovery. *Mol. Interventions* **2009**, *9*, 22−30.

(66) Hopkins, A. L.; Groom, C. R.; Alex, A. Ligand efficiency: A useful metric for lead selection. *Drug Discovery Today* **2004**, *9*, 430−431.

(67) Sharma, L. K.; Subramanian, C.; Yun, M. K.; Frank, M. W.; White, S. W.; Rock, C. O.; Lee, R. E.; Jackowski, S. A therapeutic approach to pantothenate kinase associated neurodegeneration. *Nat. Commun.* **2018**, *9*, 4399.

(68) Teague, S. J. Implications of protein flexibility for drug discovery. *Nat. Rev. Drug Discovery* **2003**, *2*, 527−541.

(69) Mysinger, M. M.; Carchia, M.; Irwin, J. J.; Shoichet, B. K. Directory of useful decoys, enhanced (DUDE-E): Better ligands and decoys for better benchmarking. *J. Med. Chem.* **2012**, *55*, 6582−6594.

(70) Shi, J.; Van de Water, R.; Hong, K.; Lamer, R. B.; Weichert, K. W.; Sandoval, C. M.; Kasibhatla, S. R.; Boehm, M. F.; Chao, J.; Lundgren, K.; Timple, N.; Lough, R.; Ibanez, G.; Boykin, C.; Burrows, F. J.; Kehry, M. R.; Yun, T. J.; Harning, E. K.; Ambrose, C.; Thompson, J.; Bixler, S. A.; Dunah, A.; Snodgrass-Belt, P.; Arndt, J.; Enyedy, I. J.; Li, P.; Hong, V. S.; McKenzie, A.; Biamonte, M. A. EC144 is a potent inhibitor of the heat shock protein 90. *J. Med. Chem.* **2012**, *55*, 7786−7795.

(71) Kamenik, A. S.; Singh, I.; Lak, P.; Balius, T. E.; Liedl, K. R.; Shoichet, B. K. Energy penalties enhance flexible receptor docking in a model cavity. *Proc. Natl. Acad. Sci. U. S. A.* **2021**, *118*, XXX.

(72) Gewirth, D. T. Paralog specific Hsp90 inhibitors - a brief history and a bright future. *Curr. Top. Med. Chem.* **2016**, *16*, 2779−2791.

(73) Mollapour, M.; Neckers, L. Post-translational modifications of Hsp90 and their contributions to chaperone regulation. *Biochim. Biophys. Acta* **2012**, *1823*, 648−655.

(74) Merski, M.; Fischer, M.; Balius, T. E.; Eidam, O.; Shoichet, B. K. Homologous ligands accommodated by discrete conformations of a buried cavity. *Proc. Natl. Acad. Sci. U. S. A.* **2015**, *112*, 5039−5044.

(75) Proia, D. A.; Bates, R. C. Ganetespib and Hsp90: Translating preclinical hypotheses into clinical promise. *Cancer Res.* **2014**, *74*, 1294−1300.

(76) Pillai, R. N.; Fennell, D. A.; Kovcin, V.; Ciuleanu, T. E.; Ramlau, R.; Kowalski, D.; Schenker, M.; Yalcin, I.; Teofilovici, F.; Vukovic, V. M.; Ramalingam, S. S. Randomized Phase III study of ganetespib, a heat shock protein 90 inhibitor, with docetaxel versus docetaxel in advanced non-small-cell lung cancer (galaxy-2). *J. Clin. Oncol.* **2020**, *38*, 613−622.

(77) Fernández-Quintero, M. L.; Vangone, A.; Loeffler, J. R.; Seidler, C. A.; Georges, G.; Liedl, K. R. Paratope states in solution improve structure prediction and docking. *Structure* **2022**, *30*, 430−440.e433.

(78) Fernández-Quintero, M. L.; Georges, G.; Varga, J. M.; Liedl, K. R. Ensembles in solution as a new paradigm for antibody structure prediction and design. *mAbs* **2021**, *13*, 1923122.

(79) Barelier, S.; Boyce, S. E.; Fish, I.; Fischer, M.; Goodin, D. B.; Shoichet, B. K. Roles for ordered and bulk solvent in ligand recognition and docking in two related cavities. *PLoS One* **2013**, *8*, No. e69153.

(80) Yang, Y.; Lill, M. A. Dissecting the influence of protein flexibility on the location and thermodynamic profile of explicit water molecules in protein-ligand binding. *J. Chem. Theory Comput.* **2016**, *12*, 4578−4592.

(81) Biela, A.; Nasief, N. N.; Betz, M.; Heine, A.; Hangauer, D.; Klebe, G. Dissecting the hydrophobic effect on the molecular level: The role of water, enthalpy, and entropy in ligand binding to thermolysin. *Angew. Chem., Int. Ed.* **2013**, *52*, 1822−1828.

(82) Breiten, B.; Lockett, M. R.; Sherman, W.; Fujita, S.; Al-Sayah, M.; Lange, H.; Bowers, C. M.; Heroux, A.; Krilov, G.; Whitesides, G. M. Water networks contribute to enthalpy/entropy compensation in protein-ligand binding. *J. Am. Chem. Soc.* **2013**, *135*, 15579−15584.

(83) Khandelwal, A.; Kent, C. N.; Balch, M.; Peng, S.; Mishra, S. J.; Deng, J.; Day, V. W.; Liu, W.; Subramanian, C.; Cohen, M.; Holzbeierlein, J. M.; Matts, R.; Blagg, B. S. J. Structure-guided design of an Hsp90β N-terminal isoform-selective inhibitor. *Nat. Commun.* **2018**, *9*, 425.

(84) Mishra, S. J.; Liu, W.; Beebe, K.; Banerjee, M.; Kent, C. N.; Munthali, V.; Koren, J.; Taylor, J. A.; Neckers, L. M.; Holzbeierlein, J.; Blagg, B. S. J. The development of Hsp90β-selective inhibitors to overcome detriments associated with. *J. Med. Chem.* **2021**, *64*, 1545−1557.

(85) Haider, K.; Huggins, D. J. Combining solvent thermodynamic profiles with functionality maps of the Hsp90 binding site to predict the displacement of water molecules. *J. Chem. Inf. Model.* **2013**, *53*, 2571−2586.

(86) Lavery, L. A.; Partridge, J. R.; Ramelot, T. A.; Elnatan, D.; Kennedy, M. A.; Agard, D. A. Structural asymmetry in the closed state of mitochondrial Hsp90 (Trap1) supports a two-step ATP hydrolysis mechanism. *Mol. Cell* **2014**, *53*, 330−343.

(87) Bergazin, T. D.; Ben-Shalom, I. Y.; Lim, N. M.; Gill, S. C.; Gilson, M. K.; Mobley, D. L. Enhancing water sampling of buried binding sites using nonequilibrium candidate monte carlo. *J. Comput.-Aided Mol. Des.* **2021**, *35*, 167−177.

(88) Graham, S. E.; Smith, R. D.; Carlson, H. A. Predicting displaceable water sites using mixed-solvent molecular dynamics. *J. Chem. Inf. Model.* **2018**, *58*, 305−314.

(89) Balius, T. E.; Fischer, M.; Stein, R. M.; Adler, T. B.; Nguyen, C. N.; Cruz, A.; Gilson, M. K.; Kurtzman, T.; Shoichet, B. K. Testing inhomogeneous solvation theory in structure-based ligand discovery. *Proc. Natl. Acad. Sci. U. S. A.* **2017**, *114*, E6839−E6846.

(90) Spyrakis, F.; Ahmed, M. H.; Bayden, A. S.; Cozzini, P.; Mozzarelli, A.; Kellogg, G. E. The roles of water in the protein matrix: A largely untapped resource for drug discovery. *J. Med. Chem.* **2017**, *60*, 6781−6827.

(91) Bolcato, G.; Bissaro, M.; Sturlese, M.; Moro, S. Comparing fragment binding poses prediction using Hsp90 as a key study: When bound water makes the difference. *Molecules* **2020**, *25*, 4651.

(92) Shadrack, D. M.; Swai, H. S.; Hassanali, A. A computational study on the role of water and conformational fluctuations in Hsp90 in response to inhibitors. *J. Mol. Graphics Modell.* **2020**, *96*, 107510.

(93) Stachowski, T. R.; Vanarotti, M.; Seetharaman, J.; Lopez, K.; Fischer, M. Water networks repopulate protein-ligand interfaces with temperature. *Angew. Chem., Int. Ed.* **2022**, *61*, e202112919.

(94) Brough, P. A.; Barril, X.; Borgognoni, J.; Chene, P.; Davies, N. G.; Davis, B.; Drysdale, M. J.; Dymock, B.; Eccles, S. A.; Garcia-Echeverria, C.; Fromont, C.; Hayes, A.; Hubbard, R. E.; Jordan, A. M.; Jensen, M. R.; Massey, A.; Merrett, A.; Padfield, A.; Parsons, R.; Radimerski, T.; Raynaud, F. I.; Robertson, A.; Roughley, S. D.; Schoepfer, J.; Simmonite, H.; Sharp, S. Y.; Surgenor, A.; Valenti, M.; Walls, S.; Webb, P.; Wood, M.; Workman, P.; Wright, L. Combining hit identification strategies: Fragment-based and in silico approaches to orally active 2-aminothieno[2,3-d]pyrimidine inhibitors of the Hsp90 molecular chaperone. *J. Med. Chem.* **2009**, *52*, 4794−4809.

(95) Wienen-Schmidt, B.; Oebbeke, M.; Ngo, K.; Heine, A.; Klebe, G. Two methods, one goal: Structural differences between cocrystallization and crystal soaking to discover ligand binding poses. *ChemMedChem* **2021**, *16*, 292−300.

(96) Yang, S.; Yoon, N. G.; Kim, D.; Park, E.; Kim, S. Y.; Lee, J. H.; Lee, C.; Kang, B. H.; Kang, S. Design and synthesis of Trap1 selective inhibitors: H-bonding with Asn171 residue in Trap1 increases paralog selectivity. *ACS Med. Chem. Lett.* **2021**, *12*, 1173−1180.

(97) Whitesell, L.; Robbins, N.; Huang, D. S.; McLellan, C. A.; Shekhar-Guturja, T.; LeBlanc, E. V.; Nation, C. S.; Hui, R.; Hutchinson, A.; Collins, C.; Chatterjee, S.; Trilles, R.; Xie, J. L.; Krysan, D. J.; Lindquist, S.; Porco, J. A.; Tatu, U.; Brown, L. E.; Pizarro, J.; Cowen, L. E. Structural basis for species-selective targeting of Hsp90 in a pathogenic fungus. *Nat. Commun.* **2019**, *10*, 402.

(98) Liebschner, D.; Afonine, P. V.; Baker, M. L.; Bunkoczi, G.; Chen, V. B.; Croll, T. I.; Hintze, B.; Hung, L. W.; Jain, S.; McCoy, A. J.; Moriarty, N. W.; Oeffner, R. D.; Poon, B. K.; Prisant, M. G.; Read, R. J.; Richardson, J. S.; Richardson, D. C.; Sammito, M. D.; Sobolev, O. V.; Stockwell, D. H.; Terwilliger, T. C.; Urzhumtsev, A. G.; Videau, L. L.; Williams, C. J.; Adams, P. D. Macromolecular structure determination using x-rays, neutrons and electrons: Recent developments in phenix. *Acta Crystallogr., Sect. D: Struct. Biol.* **2019**, *75*, 861−877.

(99) Friesner, R. A.; Murphy, R. B.; Repasky, M. P.; Frye, L. L.; Greenwood, J. R.; Halgren, T. A.; Sanschagrin, P. C.; Mainz, D. T. Extra precision glide: Docking and scoring incorporating a model of hydrophobic enclosure for protein-ligand complexes. *J. Med. Chem.* **2006**, *49*, 6177−6196.